Modeling of Fluid Shifts in the Human Thorax for Electrical Impedance Tomography

Henning Luepschen[1], Dirk van Riesen[2], Lisa Beckmann[1], Kay Hameyer[2], and Steffen Leonhardt[1]

[1]Philips Chair for Medical Information Technology, Helmholtz-Institute, RWTH Aachen University, D-52074 Aachen, Germany
[2]Institute of Electrical Machines, Chair of Electromagnetic Energy Conversion, RWTH Aachen University, D-52056 Aachen, Germany

Thoracic electrical impedance tomography (EIT) seems to be particularly useful for the monitoring of patients suffering from the acute respiratory distress syndrome (ARDS), because it is capable of detecting dynamic shifts of body fluids and lung aeration right at the bedside. EIT-derived numeric parameters would help the physician to evaluate the state of the lung more objectively. Therefore, we created a finite element method (FEM)-model of a human thorax and tested new ventilation indices regarding their ability to quantitatively describe structural changes in the lung due to the gravitationally dependent lung collapse. Additionally, we examined which current-injection electrode pair is best suited for the separation of lung and heart activity.

***Index Terms*—Acute respiratory distress syndrome (ARDS), electrical impedance tomography (EIT), finite element method (FEM) thorax model, fluid shifts, ventilation indices.**

I. Introduction

THORACIC electrical impedance tomography (EIT) is a noninvasive technique for the estimation of the spatial conductivitiy distribution in a thorax cross section. N_E electrodes (here, $N_E = 16$) are equidistantly attached to the patient's skin around the thorax. During a measurement, small alternating currents are injected into adjacent electrodes and the potentials at the remaining electrodes are measured (i.e., adjacent drive/adjacent receive). Then, they are used to reconstruct images of the change in conductivity.

In recent years, EIT has been the subject of study for a variety of clinical problems such as respiratory failure, cardiac volume changes, gastric emptying, and head imaging [1]. Even though the spatial resolution is rather low (about one tenth of the thorax diameter), EIT seems to be particularly useful for the bedside monitoring of patients suffering from the acute respiratory distress syndrome (ARDS) due to its noninvasiveness and high temporal resolution [2].

ARDS is a life-threatening state of the lung characterized by atelectasis (i.e., lung collapse) and pulmonary edema (i.e., water in the lung) and thus, variations of the conductivity distribution in the thorax. ARDS patients have to be mechanically ventilated with higher oxygen concentrations and changing pressure levels resulting in dynamic shifts of body fluids and lung aeration.

EIT is well suited for visualizing those shifts providing an instantaneous feedback to the medical staff [3], [4]. However, it still has to be examined how to further process the fast sequence of EIT images (up to 50 images/s) and how to extract and quantify the underlying physiological information in order to achieve maximum benefit. The attending physician should be able to immediately recognize ventilation changes in the lung resulting from, e.g., new ventilator settings. The evaluation would become much more objective if it were based on EIT-derived numeric parameters and not merely on visual observations of the EIT images (subtle changes are simply hard to detect). Additionally, numeric parameters will later allow an EIT-based trend analysis for different kinds of diseases.

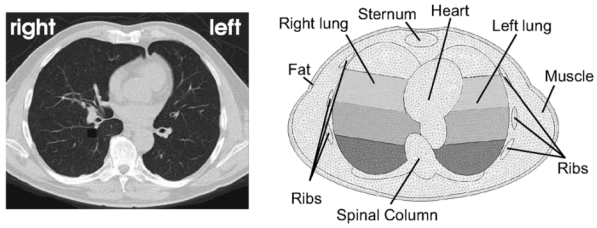

Fig. 1. (a) CT image of a human thorax and (b) corresponding 2-D-slice of the FEM-model. The three bottommost layers of the lung were subsequently filled with body fluid to simulate lung edema.

Therefore, we first created a 2+1D finite element model of the human thorax and divided the lung into four coronal layers. Then, we altered the fluid contents of the dorsal layers close to the back in order to simulate lung collapse of increasing severity. After reconstruction, we looked at different methods to quantify the given ventilation changes and compared them with the actual modifications made in the thorax model.

Finally, as EIT seems also to be capable of distinguishing between heart and lung related changes of the conductivity in the thorax [5], we examined which current-injection and voltage measurement electrode pairs are best suited for a proper separation between lung and heart activity. Hence, we calculated the average current density for the different tissues and compared them based on the position of the current injection.

II. Methods

A. Modeling

For the proper assessment of lung collapse, an adequate geometric model of the human thorax had to be created with realistic values for the electrical properties of biological tissue. Thus, we obtained the correct geometric dimensioning of the model from real CT images of a human male (see Fig. 1). The necessary simplifications made during the mesh generation were similar to the ones described in [6]. The resulting

Digital Object Identifier 10.1109/TMAG.2007.916131

TABLE I
ELECTRICAL PROPERTIES OF THE MODELED TISSUES AT 50 kHz [7]. THE ASTERISK-MARKED (*) PROPERTIES WERE USED FOR THE SIMULATION OF THE REFERENCE STATE

Tissue	Conductivity (S/m)	Rel. permittivity
Lung* (deflated)	0.26197	8,531.40
Lung (inflated)	0.10265	4,272.50
Heart*	0.19543	16,982.00
Bone* (cortical)	0.02064	264.19
Fat*	0.02424	172.42
Muscle*	0.35182	10,094.00
Body Fluid	1.50000	98.56
Blood	0.70080	5,197.70

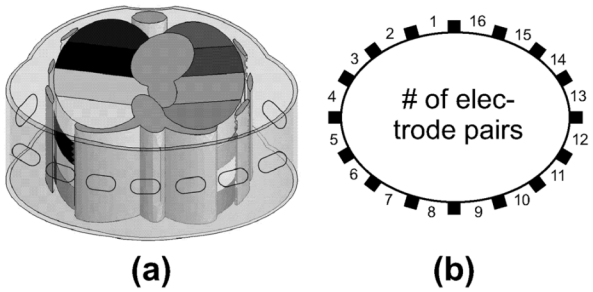

Fig. 2. (a) Electrode placement and (b) numbering of electrode pairs.

2+1D-mesh consisted of 164 000 first-order tetrahedral elements and 310 000 nodes and was created with ANSYS®.

In total, five different types of tissue were being modeled with electrical properties taken from the literature: muscle, heart, bones (spinal column, ribs, sternum), fat, and lung; cf. Table I. We decided to inject currents of 5 $\mathrm{mA_{eff}}$@50 kHz, as frequencies between 20 and 200 kHz are widely used for thoracic single-frequency EIT.

In order to simulate patient breathing, conductivity and relative permittivity of the lung were varied between deflated and inflated lung as given in [7]. Visceral movement (i.e., geometric changes) during a breath cycle was not considered as it has been reported to have a rather low influence for state-differential reconstruction algorithms [8].

Patients suffering from acute respiratory failure are usually treated in supine position. Due to the weight of its upper parts, the lung tends to collapse in the lower parts first (commonly termed as *gravitationally dependent* collapse). Therefore, we divided the lung into four coronal layers and modeled different amounts of lung collapse by subsequently replacing the three bottommost layers with collapsed lung tissue [Fig. 1(b)] without any breathing activity.

The electrical properties of the collapsed areas ($\sigma = 0.6$ S/m, $\epsilon_r = 1000$) were assumed to be a mixture of deflated lung tissue and well-conducting body fluid. This straightforward simplification should be sufficient, as mainly the missing ventilation of the collapsed lung tissue will influence the reconstructed images of conductivity change.

The electrode placement and numbering of adjacent electrode pairs can be seen in Fig. 2. For the simulation of the heart activity, we varied its electrical properties between "normal" heart and blood-filled heart (a mixture of blood and heart properties: $\sigma = 0.45$ S/m, $\epsilon_r = 11\,000$). As before, the geometric changes during a breath cycle were omitted, so that the results have a rather qualitative character.

B. Field Simulation

The field simulation was performed using iMOOSE (a FEM inhouse software package from the IEM, RWTH Aachen University, Aachen, Germany). The unknown field variable is the complex electric potential $\underline{V}$. The used formulation is given in the Galerkin form

$$\int_\Omega (\sigma + j\omega\varepsilon)\nabla\cdot\alpha_i\nabla\cdot\underline{V}\mathrm{d}\Omega = \int_\Gamma \alpha_i \underline{J}_n \mathrm{d}\Gamma \qquad \forall i = 1,\ldots,n_n. \tag{1}$$

Here, σ and ε are the conductivity and permittivity of the materials, ω is the angular frequency, and J_n is the normal current flowing into the model, which is introduced as a current density using a Neumann boundary condition. For the presented model, however, the size of the electrodes in the mesh is not constant. Using a fixed current density would lead to unwanted differing currents for each electrode position. This would not correspond well with the reality of the measurements. Thus, in the solver, the injected current density is corrected by the proper electrode size.

Simulations were conducted similar to the measuring procedure of the EIT system. For each physiological state of the lung, 16 simulations had to be carried out to account for all current-injection positions while determining the voltages between the remaining 13 electrode pairs. Hence, $N_E \cdot (N_E - 3) = 208$ voltages were determined for each state of the lung (cf. Fig. 2).

In a postprocessing step, the current density in the model was computed by

$$\underline{\vec{J}} = -(\sigma + j\omega\varepsilon)\nabla\underline{V}. \tag{2}$$

C. Image Reconstruction and Processing

State-differential EIT images $F(x,y)$ $(x,y = 1.32)$ were reconstructed from the simulated 208 voltages using the following:

1) a linear Sheffield back-projection algorithm [9];
2) a linear one-step Newton–Raphson algorithm [10].

The reconstructed images represent the conductivity changes based on either the breathing or the heartbeat activity. In order to quantify dorsoventral as well as lateral shifts of the ventilation distribution resulting from different amounts of lung collapse, we introduce a center of ventilation index y_{cog} and a ventilation ratio index $\mathrm{LR_{ratio}}$ between the left and the right lobe of the lung

$$y_{\mathrm{cog}} = \frac{\sum_x \sum_y y \cdot F(x,y)}{\sum_x \sum_y F(x,y)} \quad \mathrm{LR_{ratio}} = \frac{\sum_{x=17}^{32} \sum_y F(x,y)}{\sum_{x=1}^{16} \sum_y F(x,y)}. \tag{3}$$

The application of two different reconstruction algorithms helped to test the universal character of these indices.

To compare between lung and heart activity, we calculated the average current density for both organs

$$\underline{J}_i^* = \frac{\int_{\Omega_i} \|\underline{\vec{J}}\| \mathrm{d}\Omega_i}{\int_{\Omega_i} \mathrm{d}\Omega_i}, \qquad \text{for } i = \text{lung, heart.} \tag{4}$$

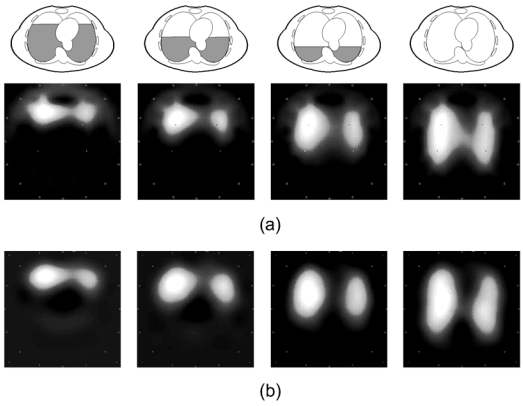

Fig. 3. Reconstructed differential EIT images for different amounts of collapsed lung with (a) the back-projection and (b) the Newton–Raphson method.

III. Results and Discussion

A. Ventilation Indices

In Fig. 3, the reconstructed images of both algorithms for different amounts of lung collapse can be seen. Up to three layers of the model were assumed to be collapsed. The images clearly show two ventilated lobes of the lung and collapsed dorsal units, even though the shapes are blurry due to the low spatial resolution. There are less reconstruction artifacts when applying the Newton–Raphson algorithm.

The center of ventilation index as given in (3) for the images of Fig. 3 is depicted in Fig. 4(a). For both reconstruction algorithms, y_{cog} increases with the percentage of ventilated lung volume. There is an almost constant offset between both methods, which might be because of the reconstruction artifacts at the upper border of the back-projected images.

In practice, however, the relative change of the ventilation distribution when adjusting, e.g., ventilator settings is much more important than the absolute value, so that the benefit of the index is independent from the applied reconstruction method.

As a consequence of the noncentral position of the heart, the volume of the left lung is smaller than the volume of the right lung for all filling states, which can also be seen in the reconstructed images of Fig. 3. The ratio between the volumes decreases if more layers are collapsed, which is nicely reflected in the $\mathrm{LR}_{\mathrm{ratio}}$ [see Fig. 4(b)].

The Newton–Raphson performs somewhat better than the back-projection algorithm as the results are closer to the identity line. If only a very small part of the lung is being ventilated, the index becomes less reliable, which can again be explained by the reconstruction artifacts and the resulting decrease in the signal-to-noise ratio (SNR).

B. Heart Activity

The ratio of the average current densities between lung (deflated and inflated, respectively) and heart tissue are depicted in Fig. 5.

The amount of current through the different tissues is obviously influenced by the position of the current-injection electrode pair. Electrode pair #5 will lead to a greater amount of current flowing through the (right) lung, whereas injection through

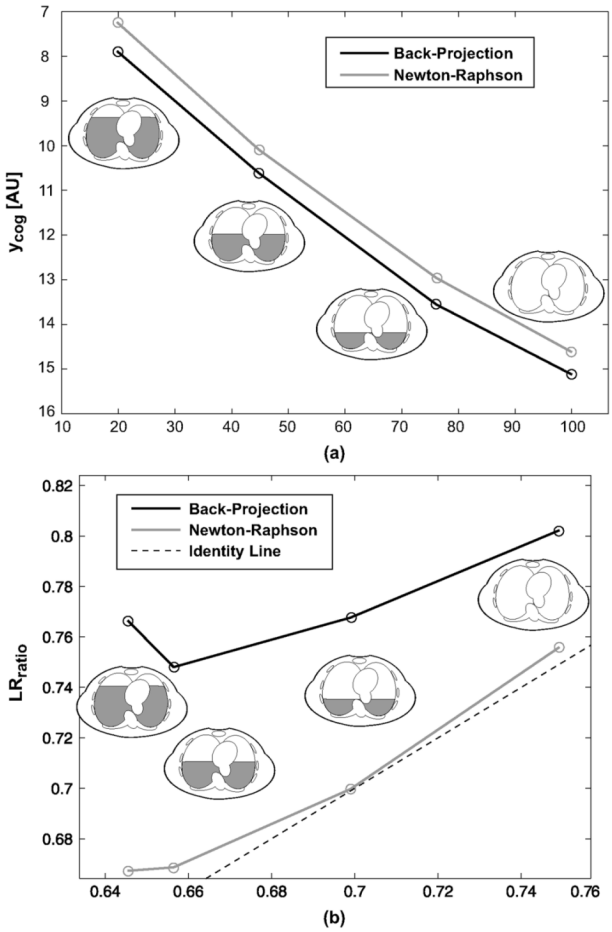

Fig. 4. (a) Center of ventilation index y_{cog} increases with the percentage of ventilated lung volume due to gravitationally dependent lung collapse. Areas shaded in gray illustrate collapsed lung tissue. (b) $\mathrm{LR}_{\mathrm{ratio}}$ is a good indicator for an unbalanced ventilation.

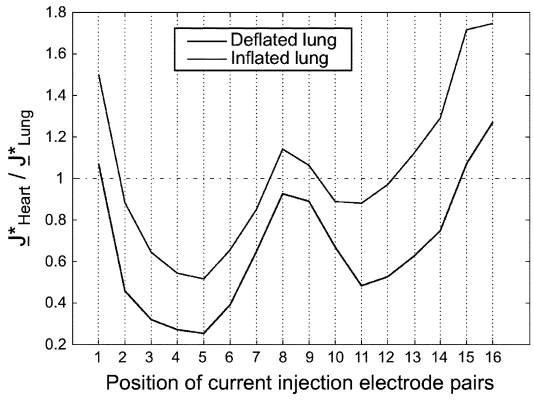

Fig. 5. Depending on the position of the current-injection electrode pair, the amount of current through heart and lung varies. For the detection of the heart activity, electrode pairs #1, #8, #9, #15, and #16 provide the best chances; see, also, Fig. 2.

electrode pair #16 maximizes the current flow in the heart. The corresponding current density images of the FEM simulations can be seen in Fig. 6.

The qualitative results for the best electrode pairs to measure the heart activity were additionally backed up by looking at the voltage changes at the boundary. Especially, when using the

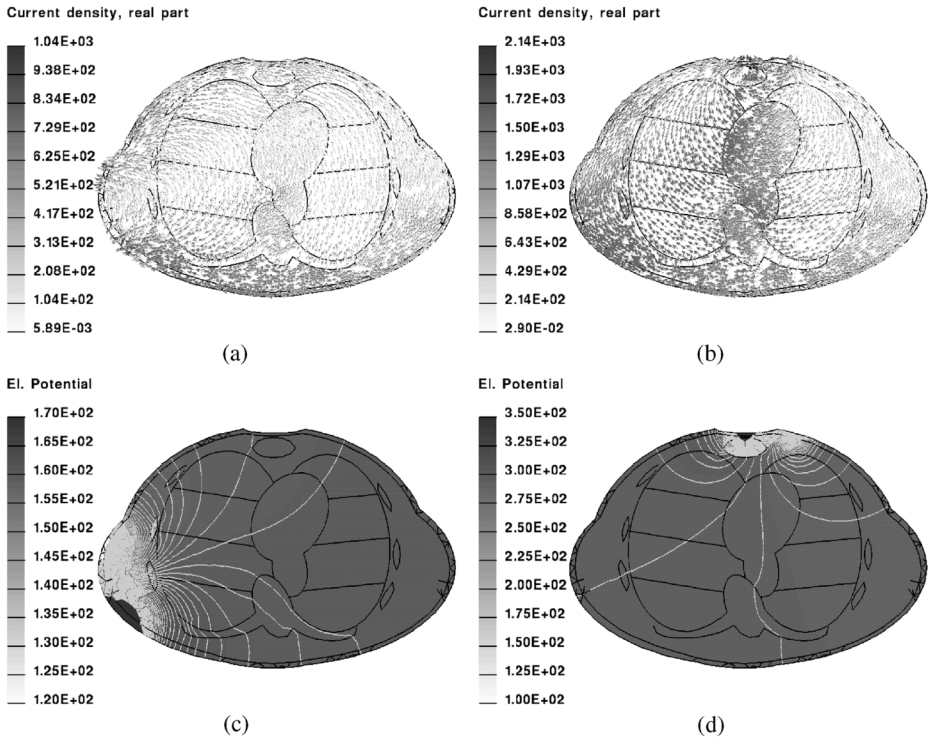

Fig. 6. Real part of the current density distribution and potential isolines from the FEM simulation for different current-injection positions.

identified optimal current-injection electrodes as receiver electrodes (e.g., current-injection pair: #16, receive pair: #8), SNR was maximized (here, the lung activity is regarded as "noise").

IV. Conclusion

Studies of the electromagnetic field distribution in the human thorax are important to learn more about the varying current paths during EIT measurements. This knowledge is necessary to verify EIT-based observations of pathological changes.

By reconstructing EIT images from the FEM simulation results of well-defined thorax geometries, we obtained reliable information about the significance and accuracy of two new ventilation indices. The center of the gravity index y_{cog} proved to be a good indicator for gravitationally dependent lung collapse. y_{cog} was almost exclusively dependent on changes in geometry and not conductivity. When simply varying the lung properties in small steps from deflated to inflated tissue without any collapse, y_{cog} changed by only 0.25%. The same applied for the LR_{ratio}, a good measure for an unbalanced ventilation, especially when using the Newton–Raphson reconstruction method.

For the detection of the heart activity, electrode pairs #1, #8, #9, #15, and #16 provide the best SNR. For these pairs, the influence of the lung activity is minimized.

For a future quantitative study, a real 3-D-model would be advantageous, because in the presented 2+1D-model the size of the heart is overestimated. Finally, a more precise modeling of the structural changes due to breathing and the heartbeat would give a better understanding of the occurring reconstruction artifacts.

References

[1] B. H. Brown, "Electrical impedance tomography (EIT): A review," *J. Med. Eng. Technol.*, vol. 27, pp. 97–108, 2003.

[2] H. Luepschen, T. Meier, M. Grossherr, T. Leibecke, J. Karsten, and S. Leonhardt, "Protective ventilation using electrical impedance tomography," *Physiol. Meas.*, vol. 28, pp. S247–S260, 2007.

[3] J. A. Victorino *et al.*, "Imbalances in regional lung ventilation—A validation study on electrical impedance tomography," *Am. J. Respir. Crit. Care Med.*, vol. 169, pp. 791–800, 2004.

[4] T. Meier, H. Luepschen, J. Karsten, T. Leibecke, M. Grossherr, H. Gehring, and S. Leonhardt, "Assessment of regional lung recruitment and derecruitment during a PEEP trial based on electrical impedance tomography," *Intensive Care Med.*, July 25, 2007, Epub ahead of print.

[5] H. Smit *et al.*, "Electrical impedance tomography to measure pulmonary perfusion: Is the reproducibility high enough for clinical practice?," *Am. J. Respir. Crit. Care Med.*, vol. 24, no. 2, pp. 491–9, 2003.

[6] O. A. Mohammed and F. G. Uler, "Detailed 2-D and 3-D finite element modeling of the human body for the evaluation of defibrillation fields," *IEEE Trans. Magn.*, vol. 29, no. 2, pp. 1403–6, Mar. 1993.

[7] Institute for Applied Physics, Italian National Research Council, "Dielectric properties of body tissue," Jun. 2007 [Online]. Available: http://niremf.ifac.cnr.it/tissprop

[8] A. Adler, R. Guardo, and Y. Berthiaume, "Impedance imaging of lung ventilation: Do we need to account for chest expansion?," *IEEE Trans. Biomed. Eng.*, vol. 43, pp. 414–420, 1996.

[9] J. Hinz *et al.*, "End-expiratory lung impedance change enables bedside monitoring of end-expiratory lung volume change," *Intensive Care Med.*, vol. 29, no. 1, pp. 37–43, 2003.

[10] J. Li, "Multifrequente Impedanztomographie zur Darstellung der Elektrischen Impedanzverteilung im Menschlichen Thorax," Ph.D. dissertation, Univ. Stuttgart, Stuttgart, Germany, Feb. 2000.

Manuscript received June 24, 2007. Corresponding author: H. Luepschen (e-mail: luepschen@hia.rwth-aachen.de).